

SPECTRALLY-RESOLVED LUMINESCENCE OF MOGANITE FROM MOGAN (GRAN CANARIA)

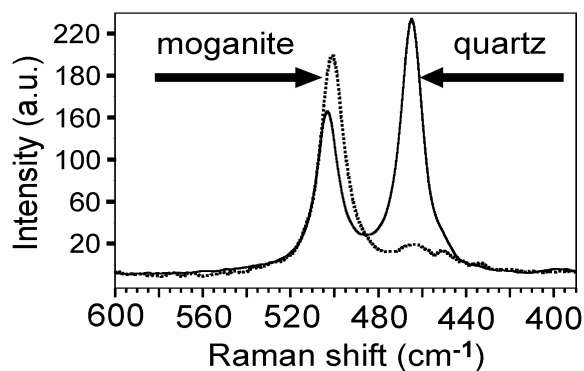
J. Garcia-Guinea^{1*}, M.A. Bustillo^{1.}, E. Crespo-Feo¹, A.A. Finch², P. D. Townsend³, D. E. Hole³, L. V. Correcher⁴.
¹Museo Nacional Ciencias Naturales-CSIC, Jose Gutierrez Abascal 2, Madrid 28006, Spain, abustillo@mncn.csic.es; ²Centre for Advanced Materials, University St Andrews, Irvine Building, St Andrews, Fife, KY16 9AL, UK, ³Science and Technology, University of Sussex, Brighton, BN1 9QH, UK., ⁴CIEMAT. Av. Complutense 22, Madrid 28040, Spain.

Introduction: Moganite mineral (SiO₂) was initially found in a near pure form in the locality-type of Mogan (Gran Canaria) [1], it was accepted as a polymorph of silica at 1999 (IMA N° 99-035). The moganite intergrowth within microcrystalline silica phases exhibits a widespread distribution at the Earth's surface. [2]. This silica polymorph contains as much as 4.5 wt.% H₂O, and 0.5 wt.% CO₂. Raman spectroscopy technique provides a measure of the moganite content in sample and its spatial variation [3]. Luminescence techniques are increasingly employed on natural silica [4], hence, it is essential to examine luminescence spectra emissions of silica aliquots, at different temperatures under different excitation agents, i.e., here, protons for ion beam luminescence (IBL), X-irradiation for radioluminescence (RL) and heating for thermoluminescence (TL), to link defects and spectra luminescence emissions.

Experimental: We study well-characterized moganite-type specimens collected by author M.A. Bustillo from fissures of rhyolitic ignimbrite flows in Mogan (Gran Canaria) [5]. Moganite rich aliquots were selected by hyperspectral Raman using a new ThermoFischer Raman Microscope with one micron spatial resolution and a laser source at 532 nm. The Electron Probe Microanalyses (EPMA) of samples were performed by a Jeol Superprobe JXA-8900M and by Environmental Scanning Electron Microscopy with X-ray Dispersive Spectrometry probe (ESEM-EDS) in aInspect-S ESEM of the FEI company. TL measurements of moganite were performed using an automated Risø TL system model TL DA-12 with an EMI 9635 QA photomultiplier and a blue filter FIB002 in which the wavelength is peaked at 320–480 nm. Spectra RL emissions were recorded in the high sensitivity spectrometer of the University of Sussex, over the 200–800 nm wavelength range during excitation of samples with 50 Gy X-irradiated employing a Phillips MG MCN 101 X-ray tube with a current of 15mA and a voltage of 25 kV. The IBL was performed under vacuum using the 3.0MeV Van der Graff accelerator facility at the University of Sussex generating a spot size of ~0.25 cm². The ion beam has a 45° offset between beam incidence and viewing angle. Light is transported by a silica fibre to a spectrometer with a cooled CCD camera. Temperature is controlled and data re-

corded at 10 degree intervals during cooling from room temperature down to 40 K [4].

Results and Discussion: Raman plots facilitates the selection of moganite-rich zones for further TL, RL and IBL analyses. Figure 1 shows two spectra taken from an hyperspectral plot, straight-line belongs to a mixed zone in where quartz (465 cm⁻¹) is more intense than moganite (502 cm⁻¹) and dotted-line is moganite richer, as the case of previous spectra CL of Mogan moganite specimens [3].



The results of the EPMA spot analysis of moganite samples shown in Table 1 do not include molecular water, hydroxyl groups, CO₂ and CO previously reported [6] in moganite samples, which can be extrapolated up ~5% of pure moganite to close the EPMA analyses. These authors reported weight losses ranges from 0.16% to 4.60%, increasing with the moganite content [6]. Table 1: Experimental EMPA analyses of Moganite samples performed in this work.

SiO ₂	94.16	95.04	94.61	94.75	94.82
Al ₂ O ₃	0.28	0.38	0.01	0.24	0.80
FeO	0.01	0.00	0.06	0.02	0.07
MnO	0.03	0.02	0.00	0.00	0.00
MgO	0.06	0.05	0.01	0.05	0.08
CaO	0.09	0.07	0.04	0.03	0.12
Na ₂ O	0.09	0.09	0.06	0.06	0.13
K ₂ O	0.03	0.07	0.02	0.02	0.11
TiO ₂	0.00	0.03	0.01	0.02	0.00
NiO	0.01	0.02	0.01	0.00	0.00
Cr ₂ O ₃	0.00	0.00	0.00	0.00	0.04
P ₂ O ₅	0.00	0.01	0.02	0.01	0.02
Cl	0.10	0.14	0.09	0.12	0.07
Total	94.86	95.92	94.94	95.32	96.26

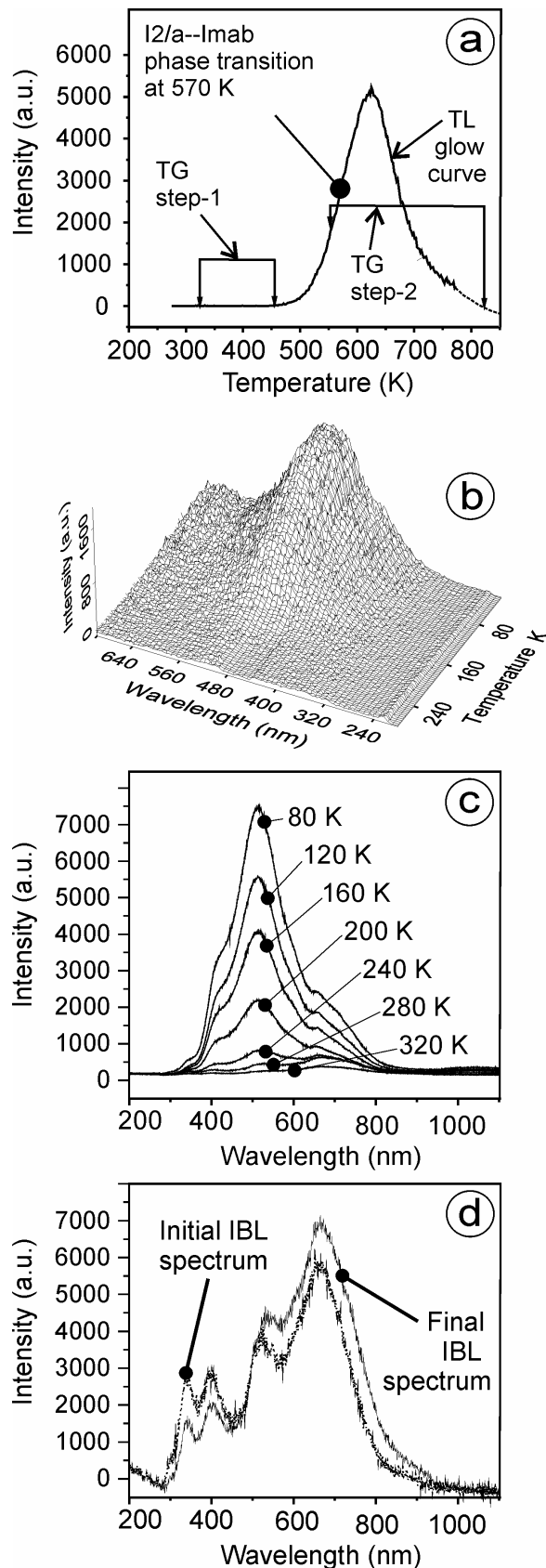


Figure 2a shows a TL glow curve at wavelength 320–480 nm of a selected fresh moganite aliquot. The TL light emission centres must be compatible with the volatile loss, i.e., water, hydroxyl groups, CO_2 and CO gases, occurred as a two steps process, with high loss rates first between 323 and 453 K and then between 553 and 823 K, previously reported in thermochemistry papers on moganite-type [6]. In addition, the reversible phase transition from space group $12/a$ to $Imab$ at approximately 570 K [7] is located in the maximum of TL light emission. Figure 2b depicts a spectra 3D RL plot of moganite-type recorded, from RT to 40K, in the high sensitivity spectrometer of the Sussex University. In accordance with the EPMA analyses and the observed spectral RL broad band, moganite seems include many of the emission-defects catalogued for SiO_2 [8], e.g., 470–500nm $[\text{AlO}_4]^\ominus$ centers, 580nm Oxygen vacancy, 620–650nm Non-bridging oxygen ions; 700nm Substitutional Fe^{3+} . During the RL measurements (Fig 1b) the lattice cryogenic stress enlarges progressively the RL emission pointing to structural defects linked with bond-breakings, and probably, with a continuous reduction in the b axis and the concomitant rotation of tetrahedra about [100] [7]. Figure 2c depicts IBL profiles of moganite from RT to 80 K with spectra positions at circa 400nm, 500nm and 700nm. In this case, the progressive cryogenic stress of the lattice enlarges also the ionoluminescence emission with a similar behaviour. Furthermore, figure 2d shows an initial IBL profile at RT using H^+ ions and a final profile after a sequential series of twenty IBL profiles at RT. This final profile shifts clearly towards the red/orange region during implantation since the dose dependence of the red/infrared emission as a function of integral dose. This peak shift can be explained in terms of changes to the coordination sphere of the activator Fe^{3+} ion caused by the ion bombardment [9].

References: [1] O.W. Flörke et al. (1976) *Zeit. Krist.* 143, 156–165, [2] P.J. Heaney and J.E. Post (1992) *Science* 255, 441–443, [3] J. Gotze, L. et al. (1998) *Contr. Miner. Petrol.* 133, 96–105, [4] T. Moxon and S. J. B. Reed (2006) *Miner. Mag.* 70, 485–498, [5] M.A. Bustillo. *J Iberian Geol.* 28, 157–166, [6] I. Petrovic et al. (1996) *Phys Chem Miner.* 23: 119–126, [7] Heaney, P.J. and Post, J.E (2001) *Amer Miner.* 86, 1358–1366, [8] M.R. Krbetschek et al. (1997) *Radiat. Meas.* 27, 695–748, [9] A. A. Finch et al. (2003) *Phys. Chem. Mineral.* 30, 373–381.

Acknowledgements. Supported by the project CGL-20008-05584-CO2-01 and Contract CSIC JAE-DOC